A pulsed electron beam time of flight apparatus for measuring absolute electron impact ionization and dissociative ionization cross sections

Ce Ma, C. R. Sporleder, and R. A. Bonham
Department of Chemistry, Indiana University, Bloomington, Indiana 47405

(Received 7 November 1990; accepted for publication 16 November 1990)

A new electron impact spectrometer has been constructed that utilizes a variable energy (4–500 eV) pulsed electron source with time-of-flight detection of electrons and ions. The apparatus can be used in a beam-beam scattering mode or in a constant pressure mode suitable for absolute measurements. A newly designed data processing system is described that uses standard CAMAC modules (LeCroy model 4208 TDCs) and allows up to 32 separate detectors to be used simultaneously in a single hit mode or up to four separate detectors in a multihit mode with each detector capable of recording up to eight hits in the same experiment. The dead time between experiments is 9.2 μs which allows up to 100 000 experiments/s for experimental flight times not exceeding 1 μs at 1 ns timing resolution. Longer flight times, up to 8.3 ms in duration, can be accommodated but with reduced timing resolution. The determination of the partial ionization cross sections for Ar^+, Ar^{2+}, and Ar^{3+} from threshold up to 500 eV is used as an illustration of some of the capabilities of the new instrument. The results obtained are in excellent agreement with other recent work for Ar^+. For the multicharged ions the cross sections were found to lie between earlier reported results. In addition the utility of the variable ion extraction field capability of the instrument is demonstrated by the separation of N^+ from N_2^{2+} for the case of electron impact dissociative ionization of N_2. A new method for placing the data on an absolute scale is presented.

I. INTRODUCTION

It has recently become apparent that absolute cross sections for nearly all kinds of electron impact scattering processes for molecules of interest to plasma processing constitute important input data for modeling calculations of plasma operating characteristics. The lack of availability of needed cross section data has been cited as an important problem.[1–4] We have designed a flexible research instrument to help alleviate this situation. A pulsed electron beam time of flight approach was selected because of our previous experience with the method[5–8] and because the use of apertures and focusing elements is held to a minimum which makes it easier to theoretically model the behavior of the system. We also believe that such an approach makes it possible to work with a larger range of ion translational kinetic energy without encountering the serious losses in transmission that seem to be characteristic of instruments employing electrostatic analyzers.[6,9] In this article we will present the design and operating characteristics of our instrument as applied to the measurement of partial ionization and dissociative ionization cross sections. New results for Ar^+, Ar^{2+}, and Ar^{3+} are given and the use of a tuneable ion extraction field is illustrated by separating two ions with the same mass to charge ratio, N^+ and N_2^{2+}, but with very different translational kinetic energy distributions. The use of a constant pressure source to make absolute measurements is also explored.

The problem of measuring partial ionization and dissociative ionization cross sections is central to the field of mass spectroscopy and there would appear to be little new to be learned from such studies. However, analytical mass spectroscopy relies on the use of calibration standards, mixtures of known composition, and not on absolute measurements.[10] Hence problems encountered with such things as ion transmission and detector efficiencies are "swept under the rug."

Standard mass spectrometers have been adopted for making absolute measurements[11–23] but the recent work of Krishnakumar and Srivastava[24] (KS) has shown that failure to correct for ion transmission losses and to optimize ion extraction efficiency can lead to very serious errors. In fact, the work of KS raises questions about the accuracy of many previous absolute measurements on multiply charged ions and ionic molecular fragments.

II. EXPERIMENTAL APPARATUS

In a previous paper we presented a number of the details concerning our new experimental facility.[25] The vacuum chamber, electron gun, and optics, Faraday trap system for monitoring the electron beam and the gas handling and pressure measuring capabilities were all discussed. For the ion experiments described below two 40 mm microchannel plate (MCP) detectors were mounted 90° and $-90°$ to the incident electron beam direction and 25 cm from the scattering center with intervening ion extraction optics as shown in Fig. 1. Note that the electron gun used in Ref. 25 was moved from its differentially pumped housing to the main vacuum chamber in order to facilitate focusing of the electron beam at low incident electron energies. Both an effusive gas jet target and a constant vacuum chamber sample gas pressure were employed in this work. One of the two detectors was biased for the detection of

 0034-6748/91/030909-15$02.00 © 1991 American Institute of Physics

Downloaded 03 Mar 2008 to 203.230.125.210. Redistribution subject to AIP license or copyright; see http://rsi.aip.org/rsi/copyright.jsp

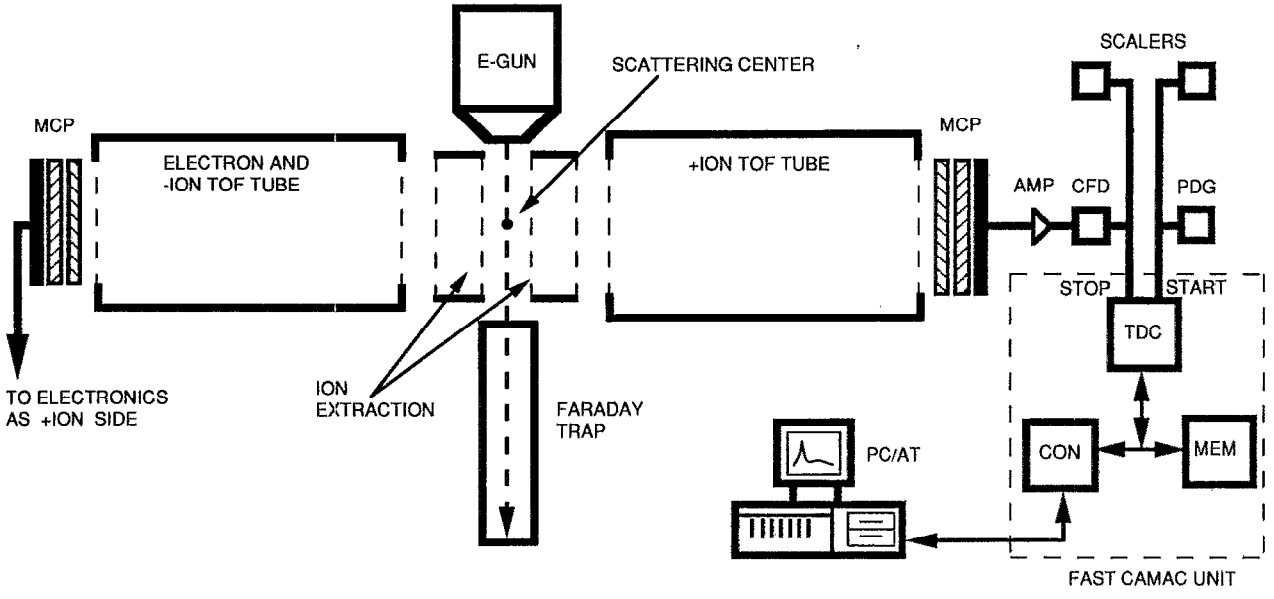

FIG. 1. Overall view of the time-of-flight ion experiment.

positive ions while the other was biased for the detection of electrons and negative ions. Hence the instrument has the capability of carrying out electron-positive ion and negative ion-positive ion coincidence experiments although this application will not be discussed in this article. The various parts of the instrument not previously presented are discussed in the following subsections.

A. Ion extraction and focusing optics

To obtain the correct intensity ratios for ion products of differing charge, initial kinetic energy, spatial position, and mass requires special attention to the ion extraction and focusing optics.[24] In order to solve these problems we were willing to sacrifice mass resolution since most molecules of interest to plasma processing are relatively light. The approach used was to employ relatively short large diameter flight tubes and detector (40-mm-diam active area) in order to minimize transmission losses. High transmission gold mesh ($91.7 \pm 0.5\%$ measured optical transmission, Buckbee-Mears, MG-8) was used to cover the ends of each cylindrical lens section in order to maintain uniform electric fields. The arrangement used is shown in Fig. 1. The distance from the scattering center to the first extraction grid is 6 mm and to the second 31 mm. The 25-mm-long aluminum cylinder with these grids covering each end could be maintained at a constant dc potential adjustable from zero to 120 V. This extraction field can be switched to ground potential, while the incident electron beam pulse is transmitted through the scattering region, for an adjustable time period from 40 ns to 1 μs. Another option that is available is to maintain the extraction optics at ground potential and switch on the extraction field after the electron pulse has passed through the extraction region. The disadvantage of this option is that the 1 μs maximum pulse duration of our pulse generator (Avtech AVR-A-1) impose an upper limit on the ion mass that can be completely detected (about mass 7). It should be pointed out that this pulser has an 8 ns rise and fall time to go along with its 0–120 V pulse amplitude and up to 100 kHz pulse repetition rate capability. Separate pulse generators of appropriate polarity were used on the positive and negative extraction grids.

After each extraction grid cylinder there is a 150-mm-long 60 mm i.d. aluminum time of flight (TOF) drift tube maintained at a constant potential which can be adjusted from zero to 1000 V. The spacing between the extraction electrode and the drift section is 6 mm. After the last grid on the back end of each TOF drift tube a detector consisting of two 40-mm-diam active area MCP detectors in a chevron arrangement was placed. An additional grid was placed between the end of the drift tube and the front surface of the MCP detector as explained in the discussion of problems given below. The front surface of each detector is maintained at a potential of 0.5–3 kV of appropriate polarity in order to insure a reasonable detection efficiency for electrons and ions. The entire configuration is surrounded by a grounded aluminum cylinder to prevent detection of background particles. All metal parts were covered with a conducting coating of colloidal graphite. The acceptance solid angle of the detector is 60° with no extraction field but sufficient drift field to insure 100% collection of all charged particles reaching the front grid of the drift tube. For neutral particles the detector acceptance solid angle is 5°.

The entire flight tube assembly constitutes an electrostatic lens whose focusing characteristic can be characterized by the ratio of the extraction voltage, V_e, to the drift tube voltage, V_{dt}. The ion trajectory simulation program SIMION[26] was employed to explore the focusing characteristics of the flight tube assembly. Trajectories for many

Downloaded 03 Mar 2008 to 203.230.125.210. Redistribution subject to AIP license or copyright; see http://rsi.aip.org/rsi/copyright.jsp

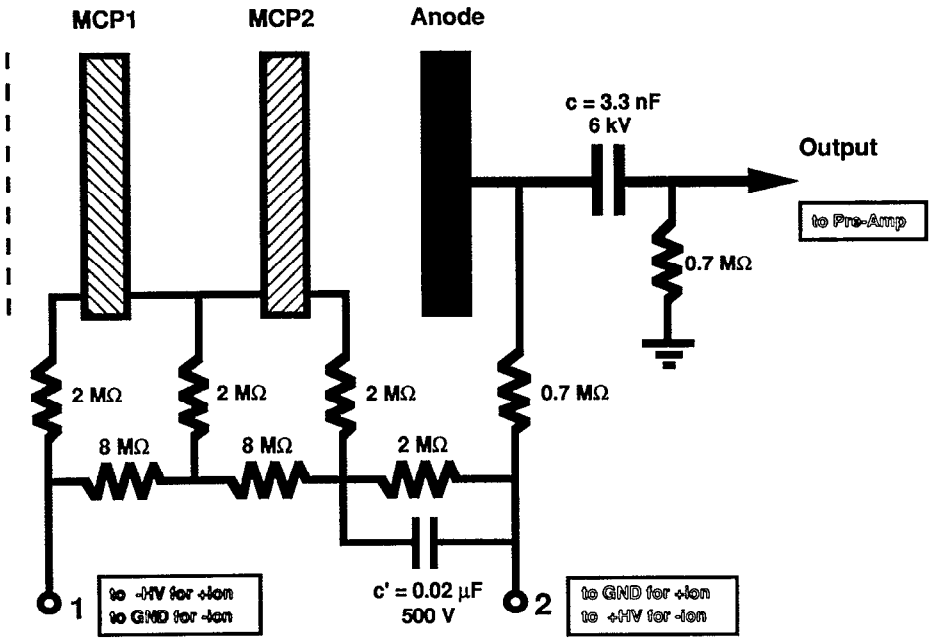

FIG. 2. MCP detectors for positive and negative particles. GND denotes ground potential or a constant bias voltage.

possible initial positions and velocities for each charge species were explored. In actual practice it was found that the optimum voltage ratio, V_e/V_{dt}, corresponded to the center of a plateau of maximum detectable ion current as a function of changing focal properties. From our experience we believe that it is essential for the design of any instrument, intended for use in making absolute cross section measurements, to have the capability of adjusting focal properties to optimize the collection efficiency for each ion separately although with our system so far we have been able to detect all ion species with maximum efficiency with the same lens setting. Our large aperture design, according to SIMION simulations, appears to be capable of detecting ions with initial translational kinetic energies up to about 10 eV with 100% collection efficiency.

One problem we have observed with this system is that for extraction voltages greater than about 30 V noise pulses are generated in the particle detectors whenever the extraction voltage is switched on and off. The problem was alleviated to some extent by the use of a larger diameter flight tube and by turning the flight tube into a giant capacitor by reducing the spacing between the outside of the flight tube and ground shield to 0.37 mm and filling the space with teflon. Except for leaving the detectors in a momentary state of saturation this problem has no effect on TOF measurements since the unwanted pulses occur at a flight time well in advance of that expected for any possible ion. The magnitude of noise pulses in our system as a function of the extraction voltage is discussed in Sec. II B. Another problem that was observed in attempts to carry out ion coincidence experiments is that whenever a positive ion hits the front surface of an MCP detector electrons are produced that are accelerated to energies of 3 keV or more in the opposite direction and reach the negative ion detector in a few ns, thus giving the appearance of a negative ion of exactly the same mass as the positive ion. It was observed that the intensity of the pseudonegative ion peak was always 0.5% of the corresponding positive ion peak. This effect can be diagnosed by simply using asymmetric drift voltages on the two sides. The flight time of the pseudo negative ion will always remain the same as the positive ion flight time with changes of 50 V or so in the drift voltage of one side relative to the other. A substantial difference in flight times would be expected if a real negative ion were involved. This problem was eliminated by installing the special bias grid, mentioned earlier, 2 mm in front of the positive ion detector and 5 mm from the end of the drift tube to suppress the electron emission.

B. Detector design and signal processing electronics

The MCP detector previously described is shown in Fig. 2. It was deemed desirable to bring as many connections to the detector outside the vacuum chamber as necessary in order to allow interchange of the positive ion detector with the negative particle detector without breaking vacuum. This allows the efficiency ratios of the two detectors to be compared for the various detected particles. It is also possible to measure relative detector efficiencies[27] since the voltage on the grid in the front of the detector can be varied without changing the voltage across the detectors. As shown, some resistors were mounted internally. The internal mount is made of machineable ceramic and the two MCP plates (Galileo, MCP-40) were held in place with springs under the nuts in order to minimize tension. The applied voltages employed in operation were about 1 kV per plate with about 250 V between the last plate and the copper anode. The output from the detector was ac coupled to an amplifier with a gain of 20 (Phillips Scientific model 775 octal pulse preamplifier) whose output was fed into a constant fraction timing discriminator (CFD) (Phillips Scientific model 715 five channel timing discrim-

Downloaded 03 Mar 2008 to 203.230.125.210. Redistribution subject to AIP license or copyright; see http://rsi.aip.org/rsi/copyright.jsp

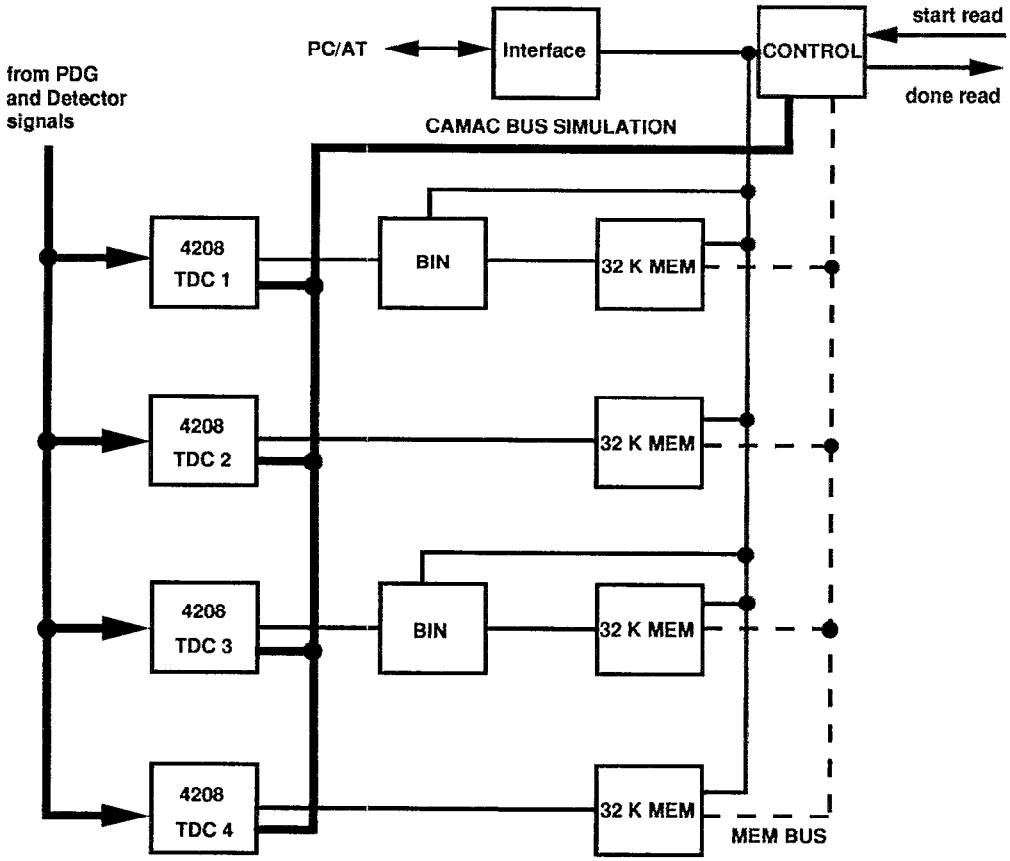

FIG. 3. A block diagram of the fast CAMAC unit (FASTMAC).

inator). A typical amplifier output for a true signal input pulse was a 200 mV negative pulse of 4 ns width. All noise pulses except those generated by the extraction field were less than 50 mV. The extraction field noise pulses were less than 50 mV for extraction fields up to 40 V. Above 40 V the extraction field noise pulses increased with increasing extraction field up to a maximum of about 90 mV at an extraction field of 120 V. This problem can be solved by either increasing the threshold level of the CFD or by starting the time-to-digital converter (TDC) after the noise pulses have passed. However tests of both approaches showed results differing by 10%–14% in the ion ratios which we believe is due to the fact that the pulse height distribution for multiply charged ions is different from that of singly charged ions. With a high threshold setting (65–95 mV) the multiple to singly charged ratios are larger which is in keeping with the view that the pulse height distributions of multiply charged ions have maxima at larger pulse height than those for singly charged species. Hence all the work reported here utilized low threshold settings and the unwanted noise pulses were eliminated by starting the TDCs about 1–2 μs after the extraction of the ions. The ion ratios were determined with lower level discriminator settings of 25 and 40 mV with no detectable difference in the values. If one wishes to measure both electrons and negative ions two TDCs are required. One is for electrons and the other, time delayed, is for negative ions since the noise pulses arrive between the signal pulses for these two species.

The output of the CFD with an appropriate setting of the lower level discriminator was a clean 50 ns wide NIM pulse, whose leading edge carried the timing information, for each true input signal pulse. The CFD has several outputs, one of which was used to feed a 100 MHz counter (LeCroy model 2551, 12 channel scaler) to record the total number of events while another was used to feed the TDC (LeCroy model 4208 real time eight channel TDC) in order to record the flight time of each event. The details of data collection are described in the next section.

C. Data collection

Since we wanted the flexibility to carry out electron scattering as well as ion experiments we needed an extended range of flight times for ion work and good timing resolution for electron experiments. The LeCroy 4208 real time TDC appeared to be the best commercial instrument available since it offered a 1 ns timing resolution over a range from -8.3 to $+8.3$ ms (23 bit resolution plus 1 sign bit). In addition it can accommodate the outputs from eight separate detectors in single hit mode or, by cascading the inputs by use of internal switches, it can accept up to eight consecutive inputs from a single detector with only 100 ps deadtime between each event. The only problem with its use in our environment was that we also required a 100 kHz experimental repetition rate for electron scattering experiments that require 900 to 1000 ns maximum flight times and in the case of ion experiments with 4–100

Downloaded 03 Mar 2008 to 203.230.125.210. Redistribution subject to AIP license or copyright; see http://rsi.aip.org/rsi/copyright.jsp

μs flight times we needed to minimize the deadtime between experiments to maximize the data collection rate. These requirements dictated a deadtime between experiments of less than 10 μs which is quite impossible to achieve by use of a standard CAMAC system.

To solve this problem we designed a special electronic bin, dubbed FASTMAC for fast CAMAC, with built in high speed memory and a logical sequencer controller which could accommodate up to four 4208 TDCs. The logical layout of the bin design is shown in Fig. 3. Circuit diagrams have been deposited with PAPS[28]. Each TDC has its own 32 k–16 bit word high speed memory. The controller was programmed with two main options called the multidetector mode option and the multihit mode option. In the multidetector mode option, reserved for use in electron scattering experiments, each detector input had its own dedicated 4 k–16 bit memory that allowed data collection at a 1 nsec timing resolution for a maximum flight time of 4 μs. The system operated as follows. An external end of experiment pulse notified the controller that it was time to unload the TDC. The controller then requested the TDC to begin its serial readout and the flight time in each of the eight channels was converted to a memory address in the dedicated fast memory. The contents of the memory at this address was then incremented by one. After the data in all eight channels had been processed the controller initiated the start of the next experiment. By trial and error it was established that the minimum time required to reliably unload the TDC was 9.2 μs; hence, we were just able to meet the design requirements for our experiment.

In the multihit mode the 32 k–16 bit word memory bank assigned to a particular TDC is not partitioned into 4 k blocks. This mode is designed for use in ion detection experiments that typically have higher count rates because of the use of an extraction field that guarantees collection of all ions produced. Up to eight inputs of a single TDC can be cascaded, by choice of the experimenter, through the use of internal switches inside each TDC. In this mode a procedure called bining is utilized by the controller to allow the experimenter to select any maximum flight time from 32 μs to 8.3 ms in steps increasing by factors of 2. This is done by reducing the timing resolution. In the 32 μs maximum flight time choice the timing resolution is 1 nsec. If one selects 64 μs the timing resolution drops to 2 ns and so on as shown in Table I. Bining is accomplished by dividing up the total maximum time in to 32 k equal sized bins and assigning each bin to one of the 32 k memory locations. Any flight time occurring in the range of a particular bin results in the contents of that memory bin being incremented by one. The implementation of this bining procedure is accomplished with no noticeable increase in the deadtime between experiments. The controller also offers the experimenter the option to use some of the TDCs in a multidetector mode and others in a multihit mode although a single TDC can operate in only one mode. It is also possible to latch the inputs of a TDC and use the multidetector mode. One only has to remember which inputs were latched so that the latched 4 k memories can be added together after the entire experiment is completed

TABLE I. Bin factors.

Number	Bin factor	Window size	Resolution
Nonbin	[a]	4.095 μs	1 ns
0	1	32 μs	1 ns
1	2	64 μs	2 ns
2	4	128 μs	4 ns
3	8	256 μs	8 ns
4	16	512 μs	16 ns
5	32	1 ms	32 ns
6	64	2 ms	64 ns
7	128	4 ms	128 ns
8	256	8 ms	256 ns

[a]This is the nonbining mode where the 32 k memory is divided into 8-4 k memory bins.

and the results are downloaded to a display computer under CAMAC control to get the total TOF spectrum for the particular detector in use. Used in this way the maximum flight time is 4 μs with 1 ns resolution. An additional feature built into our TDC controller is that it can be interrupted periodical by an external control computer (PC's LIMITED AT) through its interface to FASTMAC and the contents of its memories can be added to corresponding memories in the PC that are set up to display the overall progress of the experiment.

Initiation of an experiment takes place by the operator specifying all experimental parameters required using the PC/AT. These parameters are communicated through a GPIB IEEE-488 (National Instr. GPIB-PCIII) interface to a CAMAC crate controller (LeCroy model 8901A GPIB crate controller), a precision DVM (Keithley 197 DMM) with a homemade ten channel analog MUX, a spinning rotor pressure gauge (MKS SRG gauge), and a quadrupole mass spectrometer (Balzers QMG-125). The CAMAC crate contained two 12 channel 100 MHz scalers and two quad gate generators (LeCroy 4222 PDG). The analog MUX was used to read the outputs of the electrometer (Keithley model 642), three capacitance manometers (1-MKS 390-HA, 2-MKS 310's), and various other devices such as the output from thermocouples, ion gauges, and a flow meter.

An experiment was initiated by defining the time sequence for pulse generation using a master program on the PC/AT. Once an experiment was started the quad gate generators controlled the experimental pulse sequence by means of fast external pulses through front panel outputs and inputs to avoid the slower CAMAC internal communications. The master program also defined the data collection mode, the total number of experiments to be run and the frequency for updating the AT's data storage and display option. The updating procedure requires stopping the experiment and downloading the FASTMAC memories (45 ms). The various monitoring signals are read periodically as specified throughout the course of the experiment. A more specific description of the data collection process as it applies to the measurements reported in this paper follows.

Downloaded 03 Mar 2008 to 203.230.125.210. Redistribution subject to AIP license or copyright; see http://rsi.aip.org/rsi/copyright.jsp

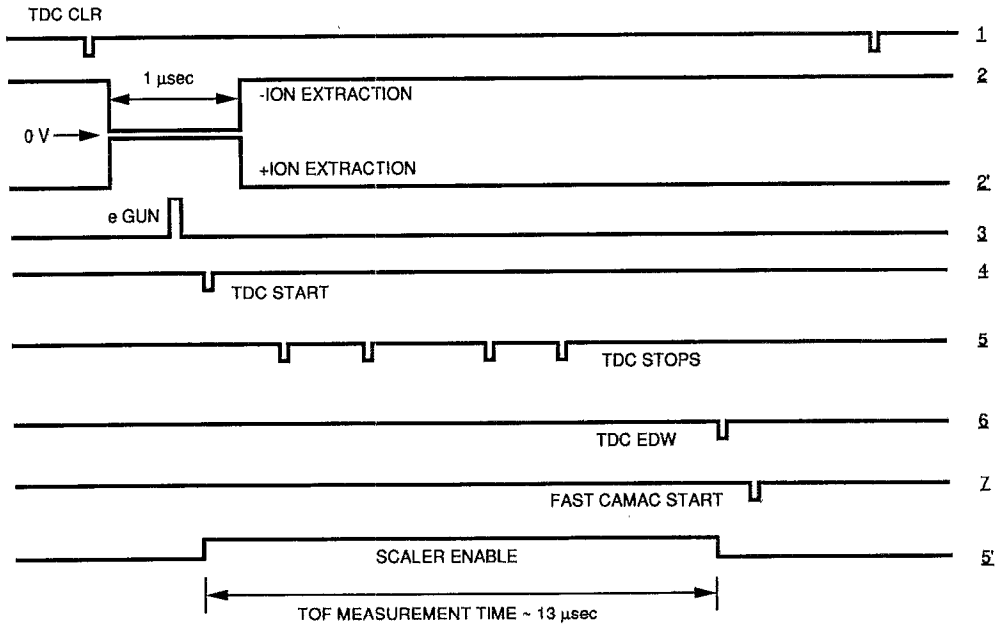

FIG. 4. Time-of-flight ion experiment timing diagram. A primed number indicates simultaneous operation with the same unprimed number.

III. EXPERIMENTAL OPERATION

For the data presented in this article an experimental repeat rate of about 30 kHz (maximum flight time of 32 μs) was employed. The procedure was initiated by an external pulse that was sent simultaneously to the trigger inputs of the two quad gate generators. The preprogrammed time delayed output pulses (1 ns resolution, 16 ms range) were used to control the experiment according

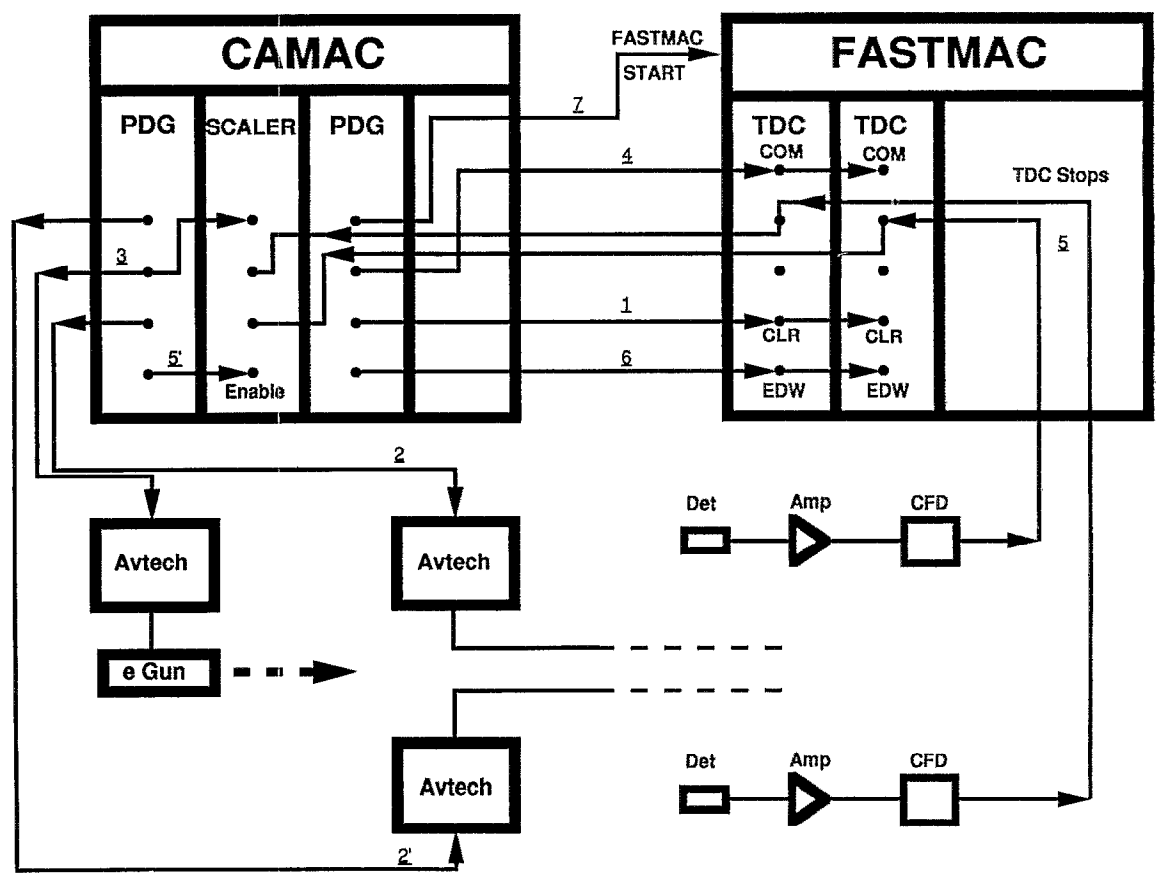

FIG. 5. A timing diagram of the pulses controlling the experiment.

Downloaded 03 Mar 2008 to 203.230.125.210. Redistribution subject to AIP license or copyright; see http://rsi.aip.org/rsi/copyright.jsp

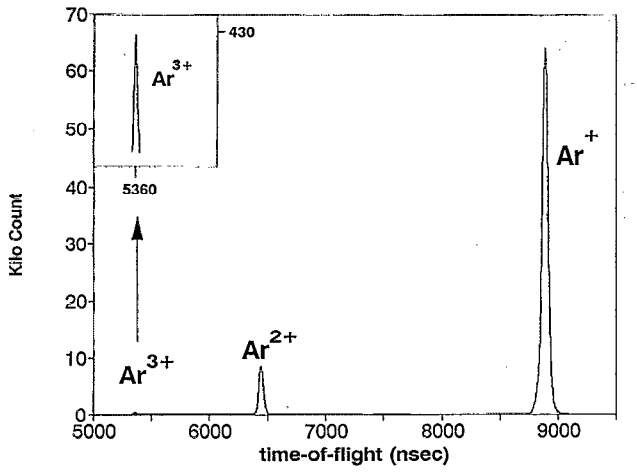

FIG. 6. Typical TOF spectrum for Argon at an electron energy of 150 eV. The vertical scale of the Ar^{3+} peak located at 5360 ns has been enlarged for better viewing.

to the timing sequence shown in Figs. 4 and 5. In Fig. 4 the time lines for pulses initiated by the quad gate generators are numbered in time order on the right. The block diagram in Fig. 5 shows how these pulses initiate the various aspects of experimental control.

Electron pulses were obtained by pulsing the control grid of the electron gun. The dc bias voltage on the control grid was at least 10 V more negative than the filament bias voltage when the gun was not being pulsed to make sure that no electrons escaped from the gun region. A pulse generator (Avtech model AVR-A-1) was used to send an adjustable 10 to 100 V high 40 ns wide positive pulse, initiated by a TTL pulse from the quad gate generator (PDG), to the control grid of the electron gun to produce the electron pulse. The unscattered portion of the electron beam was monitored by the Faraday trap.[25] The average electron beam current measured in the pulsed mode was normally in the pico Ampere range. The validity of the measurement was confirmed by comparing the ac current (pulsed mode) with the dc current. The ac current multiplied by the ratio of the ac period to the electron pulse width agreed with the dc values to 1%. It should be noted that the width of the electron beam pulse can be increased to 1 μs to increase the beam current but can be done so only with the loss of mass resolution. For electron kinetic energies less than 50 eV the electron beam energy and energy spread were measured and monitored by observing the elastically scattered electron TOF spectrum with the negative particle detector. An additional check was provided by the measurement of the appearance potentials for Ar^+ and Ar^{2+}.

For carrying out beam-beam experiments an effusive gas jet target was generated by expansion from a 0.15-mm-i.d. and 10-mm-long section of Pt hypodermic needle tubing. The flow rate was controlled by a leak valve (Granville-Phillips 203 variable leak) and monitored by a flow meter (Teledyne Hasting-Raydist NALL-10). typical

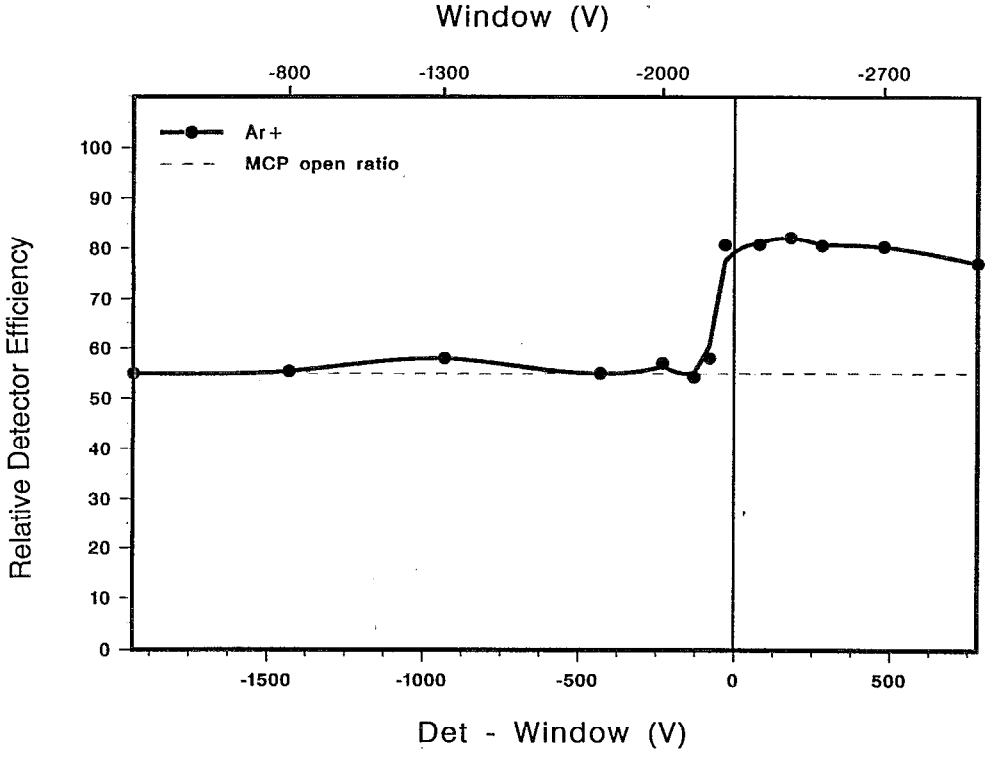

FIG. 7. The relative detection efficiency of an MCP detector as a function of the potential difference between the MCP front surface and the nearest grid. The voltage scale at the top is the actual potential of the grid while the front surface of the MCP was maintained at a constant value of -2250 V. MCP open ratio stands for the ratio of the hole area to the total active area of the MCP.

Downloaded 03 Mar 2008 to 203.230.125.210. Redistribution subject to AIP license or copyright; see http://rsi.aip.org/rsi/copyright.jsp

background chamber pressures were 1 μTorr with a flow rate of 0.1–1.0 SCCM (10^{16}–10^{17} molecules/s). A quadrupole mass spectrometer was used to monitor the residual gas. Sample purities of 99.998% for Ar and N_2 as given by the manufacturer were assumed. For operation in a constant pressure mode the gas was dumped directly into the large vacuum chamber through a 6-mm-i.d. stainless steel tube and the flow was adjusted by means of the adjustable leak until a desired pressure was obtained. We found that this simple procedure, after about a 30 min stabilization period, yielded a constant pressure environment to better than $\pm 0.5\%$ variation/h as determined by our SRG gauge. The absolute chamber pressure was determined by comparing our SRG gauge with our capacitance manometers at a pressure of 10^{-2} Torr. The residual drag offset of the SRG was determined when the system was pumped down to 10^{-8} Torr for each gas target. The manufacturers calibration of the capacitance manometer and the linearity of both instruments at lower pressures were assumed. A direct comparison was carried out between the two types of gauges down to pressures of 10^{-4} Torr. Chamber pressures in the range 10^{-6}–10^{-4} could be measured and maintained in this way.

After an adjustable period of 50 to 200 ns after the electron pulse passed through the scattering region the previously actuated pulse that shorted the dc extraction field to ground potential was turned off and ion extraction was initiated. Detector output signals were processed as described previously. A TDC with seven of eight channels cascaded was used with each detector while the total count rate of each detector was simultaneously monitored with a 100 MHz scaler. Measurements were first made with a maximum flight time of 32 μs and 1 ns resolution as a spectral survey. For the data collection scans a 13 μs maximum flight time was usually employed for the experiments reported here. At the end of an experiment one of the PDG NIM outputs was programmed to send an end-of-window (EDW) pulse to the TDCS to disable all the inputs. One μs after the EDW pulse a TTL pulse from the quad gate was sent to the FASTMAC unit which then issued a CAMAC read command through the CAMAC bus which initiated the TDCs serial readouts into their dedicated FASTMAC memories. The accumulated TOF spectra were transferred to update the PC's memory at periods of 1–30 min. Upon completion of the data transfer the PC initiated a FASTMAC memory clear and returned control of the experiment to the quad gates. A typical TOF spectrum is shown in Fig. 6 for Ar at an incident electron energy of 150 eV.

The experimental measurements on Ar were carried out by first establishing the ion current ratios $[I_{Ar}^{2+}/I_{Ar}^{+}](E)$ and $[I_{Ar}^{3+}/I_{Ar}^{+}](E)$ as a function of electron impact energy, E, from threshold to 500 eV by making measurements over 2 to 20 h with a statistical accuracy of better than 0.5%. Note that the ratios are independent of variations in most experimental parameters with time. The relative scale and hence the shape of the Ar^+ partial ionization cross section was next established by counting Ar^+ events for 1 min intervals at a selected value of the electron impact energy. As a check on the constancy of experimental conditions the Ar^+ count rate for an impact energy of 80 eV was recorded before and after the measurement of each new energy point. Variations between the two 80 eV measurements was found to always be less than 0.7%. The average of the two 80 eV ion currents, I_{norm} (80 eV), was then used to define the relative partial Ar^+ cross sections, $\sigma_{\text{rel}}^{Ar^+}$, as

$$\sigma_{\text{rel}}^{Ar^+}(E) = I_{Ar} + (E)/[I_e I_{\text{norm}}(80\ \text{eV})], \tag{1}$$

where E is the electron impact energy for the point in question, $I_{Ar}^{+}(E)$ is the Ar^+ ion current at the energy E, and I_e is the average electron beam current over the time span defined by the two 80 eV measurements. The gas beam intensity variations as inferred from background pressure measurements and pushing pressure measurements was found to change by less than 0.5% and no correction was applied.

IV. ABSOLUTE SCALE DETERMINATION

The relative scale was normalized to an absolute scale by two different procedures. Because of the existence of the accurate total cross section measurements of Rapp and Englander-Golden (REG)[29] the most accurate approach for normalization appears to be to define the absolute total ionization cross section as

$$\sigma_{\text{tot ion}}(E) = C_0 \sigma_{\text{rel}}^{Ar^+}(E)\{1 + 2[I_{Ar}^{2+}/I_{Ar}^{+}](E) + 3[I_{Ar}^{3+}/I_{Ar}^{+}](E)\}, \tag{2}$$

where C_0 is a normalizing constant defined as

$$C_0 = \sigma_{\text{REG}}(E)/\{\sigma_{\text{rel}}^{Ar^+}(E)[1 + 2(I_{Ar}^{2+}/I_{Ar}^{+})(E) + 3(I_{Ar}^{3+}/I_{Ar}^{+})(E)]\}|_{E=80\ \text{eV}}, \tag{3}$$

with σ_{REG} the Rapp Englander–Golden result and all incident energies, E, are 80 eV. The absolute partial ionization cross sections are then given by

$$\sigma_{Ar}^{+}(E) = C_0 \sigma_{\text{rel}}^{Ar^+}(E), \tag{4}$$

$$\sigma_{Ar}^{2+}(E) = C_0 \sigma_{\text{rel}}^{Ar^+}(E)[I_{Ar}^{2+}/I_{Ar}^{+}](E), \tag{5}$$

and

$$\sigma_{Ar}^{3+}(E) = C_0 \sigma_{\text{rel}}^{Ar^+}(E)[I_{Ar}^{3+}/I_{Ar}^{+}](E). \tag{6}$$

A second procedure for normalization, transmission method, was developed that was less accurate but did not depend on previous total ionization cross section measurements and can be employed in cases where total ionization cross sections are unavailable. In this case the entire vacuum chamber was filled with gas by balancing the pumping speed against the inlet leak rate and the pressure was measured as described above. The manufacturers calibration and linearity of the MKS gauge below the lowest calibration pressure were assumed. Constancy of the gas dependent correction and linearity to lower pressures was also assumed for the SRG gauge. The measured ion current for Ar^+ at an incident electron energy E_o is then given as

Downloaded 03 Mar 2008 to 203.230.125.210. Redistribution subject to AIP license or copyright; see http://rsi.aip.org/rsi/copyright.jsp

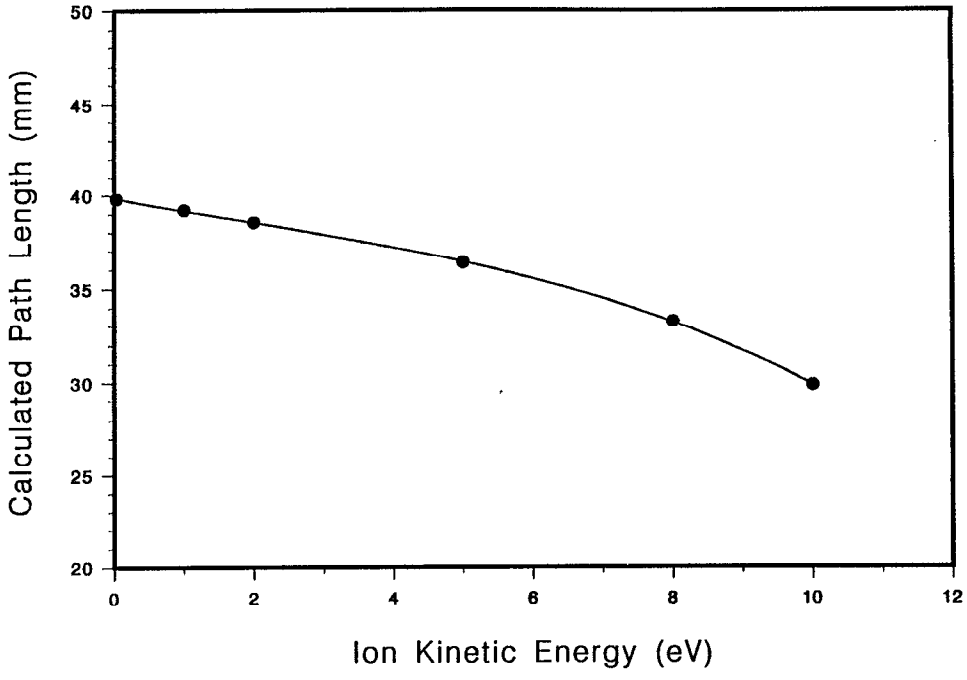

FIG. 8. The calculated scattering length l as a function of initial ion kinetic energy.

$$I_{\mathrm{Ar}^+}(E_0) = \epsilon I_F n l \sigma^+_{\mathrm{Ar}}(E_o) \exp\{-n[\langle L\sigma_{\text{ion-mol}}\rangle - L'\sigma_{\text{tot}}(E_o)]\}, \quad (7)$$

where ϵ is the absolute detector efficiency including all losses in the ion transmission optics, I_F is the electron beam current measured in the Faraday trap during the course of the experiment, n is the number density of the gas, l is the path length as viewed by the detector from which the ions are extracted, $\sigma^+_{\mathrm{Ar}}(E_o)$ is the sought after absolute cross section for Ar^+ at an electron impact energy E_o, and $\langle L\sigma_{\text{ion-mol}}\rangle$ is the energy averaged product of the ion flight distance to the detector, L, times the ion-molecule total collision cross section, $\sigma_{\text{ion-mol}}$, L' is the distance from beginning of the viewing range of the ion detector (the end closest to the electron gun) to the Faraday trap entrance, and σ_{tot} is the total electron scattering cross section at the electron energy E_o. The idea here is to obtain the total Ar^+ ion current as a function of the number density of the gas. From such data it is possible to extract the product $\epsilon l \sigma_{\mathrm{Ar}^+}$. The greater uncertainty involved in this method arises principally from our lack of knowledge of the detector efficiency and the path length. The optical transmission of the grid system was $64 \pm 1\%$ from measuring the attenuation of a light beam passing through the grids. Computer simulations indicated that electric field induced variations of the transmission from the optical value should be less than 5%. Gao *et al.* found that the detector efficiency was 60% and independent of ion mass or translational kinetic energy above 3 kV[30] for H^+, He^+, and O^+. Using SIMION we were able to show that positive ions can be detected only if they hit the holes of the MCP if the potential on the MCP surface was lower then the potential on the screen in front of the detector. By varying the potential between the MCP and the screen we were able to measure the relative efficiency of the MCP detector as shown in Fig. 7. Note that the efficiency is constant as long as the field sucks electrons away from the front face of the MCP detector and sharply rises by about 33% as the field becomes attractive and secondaries produced on the front face of the MCP are collected back and presumably focused down the holes. Our picture of the MCP efficiency is that as long as positive ions are strongly accelerated into the front face of the MCP all secondary electrons produced by front face collisions will be pulled backwards from the plate and the absolute efficiency will just be the ratio of the hole area to the total area of the MCP providing that the ion impact energy is high enough to guarantee that each ion entering a hole has a 100% counting efficiency. It should be noted that the sharp increase of the efficiency as the field becomes attractive to electrons actually starts slightly before the field becomes attractive, possibly due to the fact that the potential in the holes is attractive to electrons, and rises to a maximum in about the same way as secondary electron production curves for ion impact.[31] Because of these observations and the previous absolute efficiency calibrations of MCP plates we believe that the absolute efficiency of an MCP used with a 2–3 kV positive ion acceleration potential immediately in front of the MCP surface should be the ratio of the open area to the total area of the active portion of the plate. We have obtained backscattering electron microscope images of our MCPs at a resolution of 20 μm/cm and have estimated the efficiency of our plates to be 0.55 ± 0.01 from

Downloaded 03 Mar 2008 to 203.230.125.210. Redistribution subject to AIP license or copyright; see http://rsi.aip.org/rsi/copyright.jsp

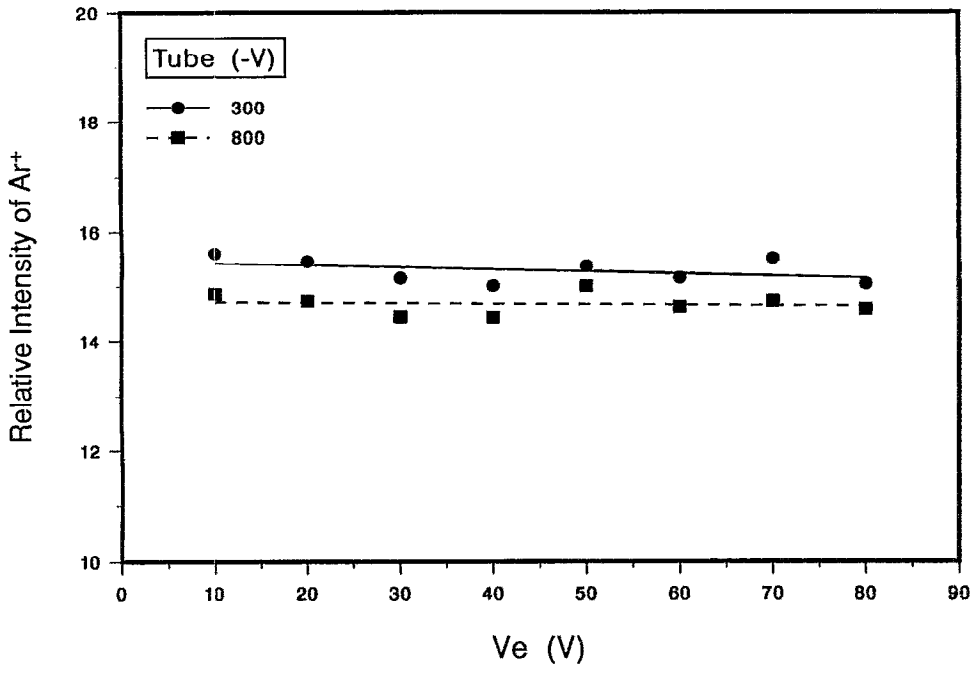

FIG. 9. Ion count rate as a function of the extraction field for drift tube potentials of 300 and 800 V.

area measurements in good agreement with the manufacturers specification of 0.55.

The average path length l was calculated from trajectory calculations using SIMION. One half the effective path length, $l/2$, was determined by finding the largest value of r_i along the length of the electron pulse track through the gas starting from $r_i = 0$ at the scattering center at which one of six initial orthogonal ion velocities leads to a calculated ion trajectory which fails to make its way to the detector. For each position, r_i, a trajectory for an ion leaving the track at each of the six initial ion velocity directions for an initial ion kinetic energy E_o was calculated. The six different perpendicular directions leaving each point r_i were chosen as follows. The motion of the four ion tracks with initial velocity vectors perpendicular to the gas nozzle direction, with two of the vectors parallel to the extraction cylinder axis, were constrained to a plane containing these vectors. The remaining two were assumed equivalent and only the trajectories of one, assumed to lie in a plane containing the gas nozzle direction, and the TOF drift tube symmetry axis, were computed. The gas nozzle, although withdrawn in the experiments, is used here only as an indication of orientation. In Fig. 8 a plot of effective path length, $l(E_o)$, as a function of the initial ion energy E_o is given based on this definition. For ions with room temperature translational kinetic energies the effective path is close to the geometric path length, 40 mm, as determined by the size of the extraction screen. For hot ions the effective path decreases but does so in almost a linear fashion. Hence if the translational kinetic energy distribution is symmetric about some average value we can expect l to be given by the average value. As a check on these calculations we measured the ion current for Ar^+ as a function of the extraction voltage from 10 V up to 80 V for drift voltages of 300 and 800 V. The results are shown in Fig. 9 and indicate virtually no significant change in ion current over the range studied which is in keeping with our assumption that the average path l, taken as 39 mm for Ar gas from the calculation, is very close to the geometric value. Obviously for ions with several eV of translational kinetic energy the situation must be carefully studied and the slowest ion in the mass spectrum should be selected as the calibration species.

V. DETERMINATION OF TRANSLATIONAL KINETIC ENERGY

While the determination of translational kinetic energy of the fragments was not one of the primary design requirements it was pleasing to find that the instrument was fairly sensitive to it. An illustration of this application is shown in Fig. 10 for 150 eV electron impact on N_2. The TOF spectrum in the region of the N^+-N_2^{2+} peak is shown as a function of extraction voltage. At the top of the figure, for an extraction field of 40 V, a single peak is observed since both species have the same mass to charge ratio. As the extraction field is reduced one can observe the separation of the peak into two peaks, one broad and one narrow. It would appear reasonable to assume that the sharp peak at longer flight times contains the N_2^{2+} contribution and that the broad peak at shorter flight times is almost certainly due to N^+. We cannot rule out a contribution to the sharp peak area from slow N^+ and, in fact, in the lowest scan in the figure at an extraction voltage of 1 V it appears that the N^+ peak does indeed have a low energy tail. We have also observed the N^+ and N_2^{2+} components at zero extraction

Downloaded 03 Mar 2008 to 203.230.125.210. Redistribution subject to AIP license or copyright; see http://rsi.aip.org/rsi/copyright.jsp

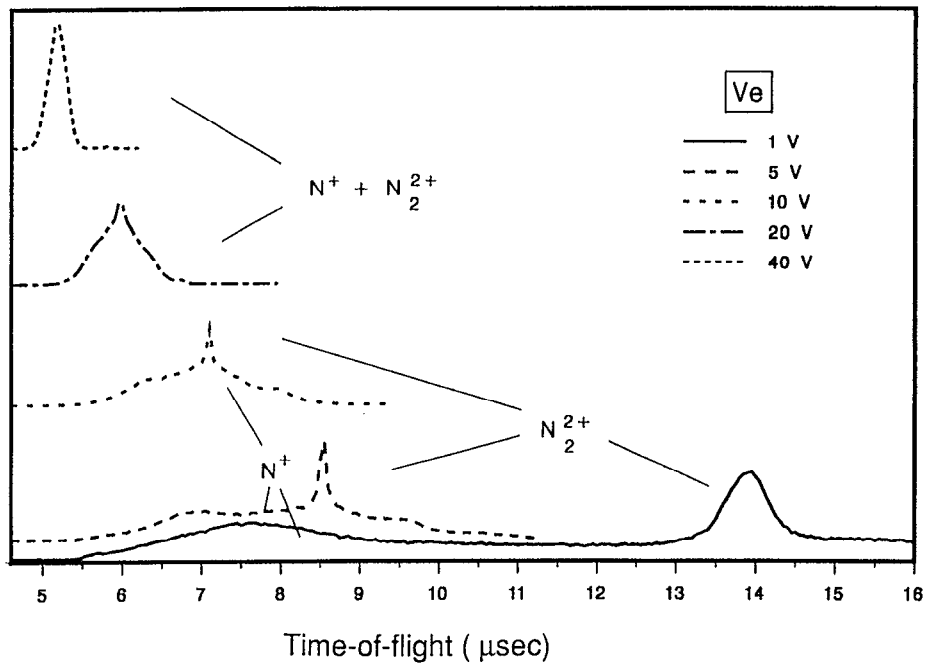

FIG. 10. TOF spectra of N^+ and N_2^{2+} as a function of the extraction field.

field where the N_2^{2+} peak occurs at a flight time of about 2 ms. We believe that the observations observed here can be used to back out the kinetic energy distributions of the various ions by means of trajectory calculations using SIMION. It is not a simple problem however as the extraction efficiency decreases with decreasing extraction field and at zero extraction field one is measuring the angular dependence of the ion emission at 90° to the electron beam direction averaged over the acceptance cone of the detector. Obviously if the primary goal were to measure this

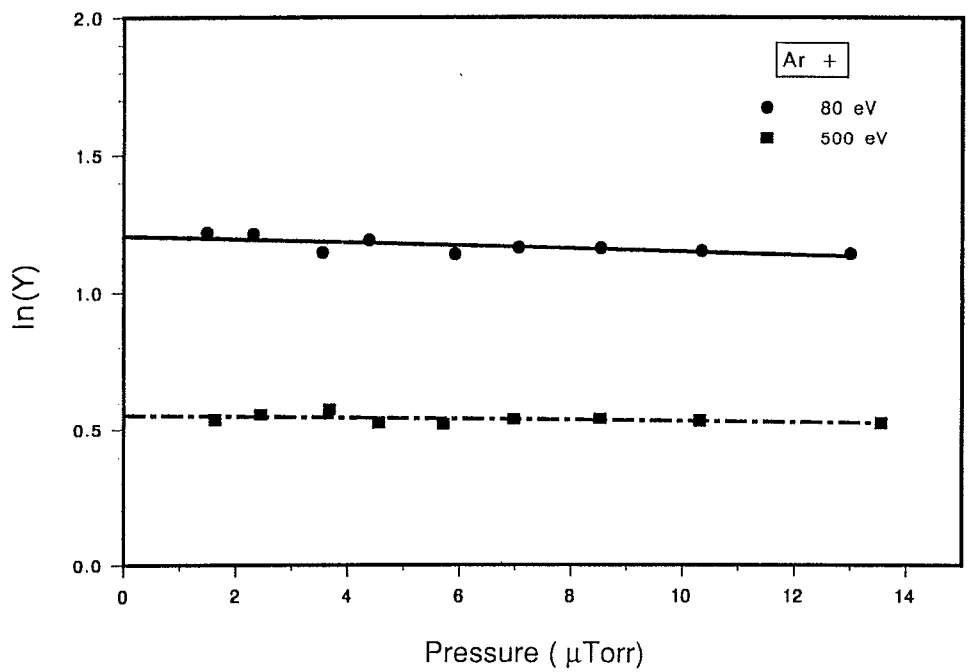

FIG. 11. A plot of $\ln(Y)$ vs pressure where Y is the ratio of ion current to the product of Faraday trap electron current and pressure. The upper curve is for an electron impact energy of 80 eV and the lower for 500 eV.

Downloaded 03 Mar 2008 to 203.230.125.210. Redistribution subject to AIP license or copyright; see http://rsi.aip.org/rsi/copyright.jsp

TABLE II. Present results of the absolute partial ionization cross sections for Ar in units of Å^2.

Energy (eV)	Ar^+ (×1)	Ar^{2+} (×10)	Ar^{3+} (×1000)
20	0.55	...	...
25	1.26	...	...
30	1.75	...	...
35	2.09	...	...
40	2.31	...	...
45	2.42	0.02	...
50	2.48	0.12	...
55	2.49	0.45	...
60	2.48	0.91	...
65	2.48	1.38	...
70	2.51	1.68	...
75	2.50	1.85	...
80	2.50	1.98	...
85	2.49	2.06	...
90	2.49	2.09	...
95	2.48	2.11	0.48
100	2.47	2.15	0.74
105	2.46	2.19	1.72
110	2.45	2.22	2.45
115	2.43	2.22	3.41
120	2.42	2.21	4.12
125	2.41	2.20	4.81
130	2.39	2.18	5.26
135	2.37	2.16	5.69
140	2.35	2.15	6.12
145	2.34	2.13	6.31
150	2.32	2.11	6.72
160	2.28	2.05	7.06
170	2.23	1.96	7.15
180	2.19	1.88	7.23
190	2.15	1.82	7.29
200	2.10	1.77	7.14
225	1.98	1.61	6.74
250	1.87	1.46	6.34
275	1.75	1.33	5.79
300	1.65	1.23	6.11
350	1.48	1.06	7.10
400	1.36	0.95	7.73
450	1.28	0.86	8.19
500	1.22	0.78	8.42

angle dependent cross section a multiple detector array with smaller detector acceptance angles would be preferable.

VI. ERROR ANALYSIS

The error estimate for the absolute partial ionization cross sections was arrived at by considering the uncertainties involved in each of the experiments carried out to reach the final results and are presented below.

A. Error in the ion ratio measurements

The ion current ratios should be independent of variations in the gas beam density or electron beam current. The statistical counting uncertainties for Ar^+, Ar^{2+}, and Ar^{3+} were 0.05%, 0.2%, and 0.7%, respectively, at each incident electron energy except for points very close to their ionization threshold. The work reported in Ref. 30 indicated that the efficiencies of H^+, He^+, and O^+, using an MCP detector similar to ours, were the same to within 5% over a wide range of ion impact energies. Another absolute efficiency calibration using Mg^+ showed a different energy dependence of the efficiency correction but the efficiency for an ion kinetic energy of 2–3 keV was about 0.6.[32] Based on these works we have assumed that our detector efficiencies are identical for all ions to within 6%. We have also assumed that our ion extraction efficiencies were 100% for each ionic species. We varied the extraction field focusing to establish that a plateau existed for the maximum ion current of each species for a range of extraction potential and drift voltage values. No error was assumed for the extraction efficiency but it should be noted that our measurements constitute a lower bound for this effect since it is believed that any problem with the extraction efficiency would be less serious for the multiply charged states. The error estimated for the Ar^{2+} and Ar^{3+} current ratios was 6% and 7%, respectively.

B. Error in the determination of the Ar^+ cross section shape

The statistical error in $I_{\text{norm}}(E)$ was maintained at better than 0.35%. The reproducibility of the Ar^+ ion current measurements at 80 eV taken before and after each measurement at the energy E was better than 0.5%. This was taken as the uncertainty estimate for variations in the electron and gas beams. The uncertainty in the measurement of I_e was taken as the manufacturers specified uncertainty of 1.3% for the pico Ampere scale of the Keithley 642 electrometer. The Faraday trap that has an aspect ratio of 100 to 1 was assumed to be 100% efficient for all energies. The incident electron beam was scanned across the front face of the trap to establish that the entire electron beam was being collected. The error from this source was assumed to be less then 0.5% and will be more serious at lower electron impact energies where the electron beam cannot be focused as tightly. We estimate that the error in our determination of the shape of the Ar^+ ionization curve is of the order of 2%.

C. Error from the normalization procedures

For the normalization to the results of Ref. 29 we used the uncertainty of 7% assigned by these authors to their work. This yields an overall uncertainty estimate of about 8% for all three cross sections reported.

For the absolute scale determination by use of a transmission experiment the uncertainties in the measured grid transmission was estimated to be 1%, an additional 5% was assumed to account for possible field effects on the grid transmission, the absolute ion efficiency uncertainty was estimated at 10% and the effective path length error was estimated conservatively to be 10%. The latter uncertainty was chosen since our experience with SIMION has been that experimental predictions using it have always agreed with observation to better than 10%. The number density was estimated to have a 3% uncertainty based on our previous total cross section work.[25] The uncertainty in the

Downloaded 03 Mar 2008 to 203.230.125.210. Redistribution subject to AIP license or copyright; see http://rsi.aip.org/rsi/copyright.jsp

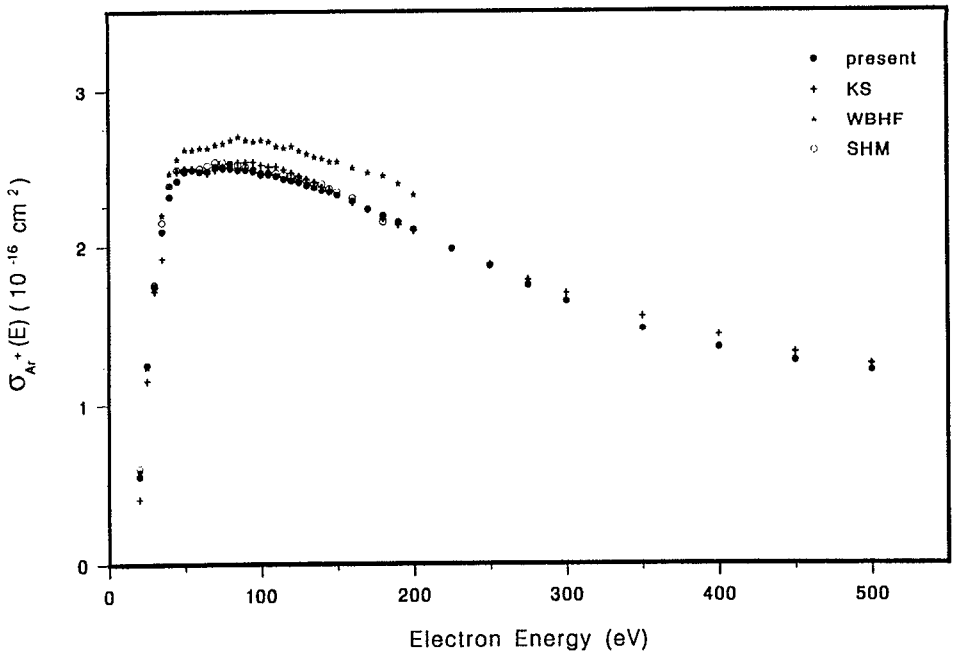

FIG. 12. The partial ionization cross section (PICS) for Ar^+ from 20 to 500 eV. Present: this work, KS: Ref. 14, WBHF: Ref. 13, and SHM: Ref. 11.

incident electron beam current was taken as 1.3% as explained in the paragraph above. The statistical and other uncertainties in the measured Ar^+ ion current were taken as 1%. The overall uncertainty was estimated at around 15%. Figure 11 shows a plot of the natural log of the ratio of the ion current to number density versus gas pressure for incident electron energies of 80 and 500 eV. The straight line behavior is a necessary condition for this analysis to be valid. The uncertainty in the intercept $\ln[\epsilon l \sigma_{Ar^+}]$ was found to be 0.6% as determined by least squares analysis of the data.

VII. EXPERIMENTAL RESULTS FOR Ar

In Table II we give the values for the absolute partial ionization cross sections for Ar^+, Ar^{2+}, and Ar^{3+} as a

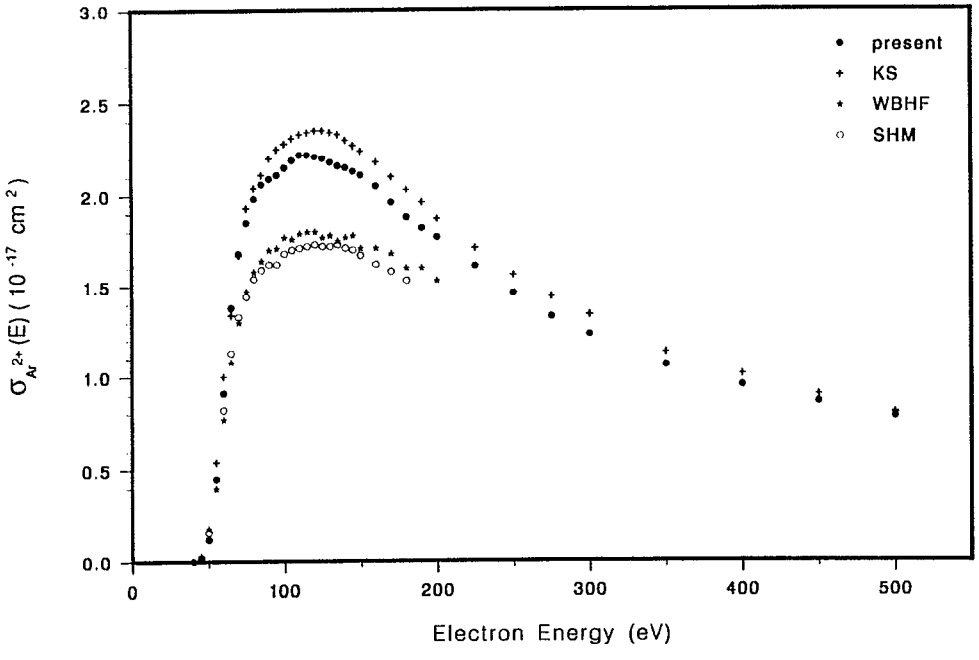

FIG. 13. The partial ionization cross section (PICS) for Ar^{2+} from 45 to 500 eV. Present: this work, KS: Ref. 14, WBHF: Ref. 13, and SHM: Ref. 11.

Downloaded 03 Mar 2008 to 203.230.125.210. Redistribution subject to AIP license or copyright; see http://rsi.aip.org/rsi/copyright.jsp

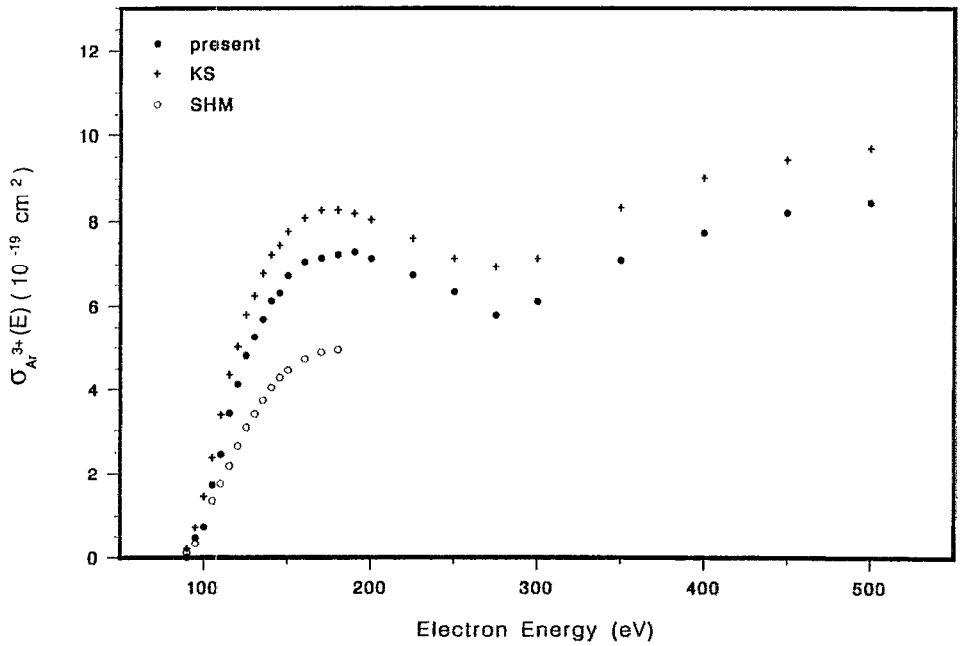

FIG. 14. The partial ionization cross section (PICS) for Ar^{3+} from 95 to 500 eV. Present: this work, KS: Ref. 14, and SHM: Ref. 11.

function of electron impact energy from threshold up to 500 eV. The absolute scale of the present work was determined by the transmission experiment discussed above. In Table II the results for Ar^+ are given for an absolute normalization based on the average of the absolute scale determinations at 80 and 500 eV using the constant chamber pressure transmission method. The deviation between the two scale determinations was 7%. In Figs. 12–14 our results are compared with those most recently obtained in other laboratories. A good review for the older results was given in Ref. 24. For Ar^+, Fig. 12, our results are in excellent agreement with those of KS[24] and SHM[21] and lie below those of WBHF[23] which may be high due to the presence of excited states in the fast neutral beam employed by these authors although the differences are well within the quoted experimental uncertainty. In Fig. 13 our results are in agreement with those of KS to better than 8% but in serious disagreement with those of SHM and WBHF. In the case of Ar^{3+}, Fig. 14, our results are as much as 40% higher at 180 eV than those of SHM but 15% lower than those of KS. The results from WBHF are not available for Ar^{3+}. The reasons for these observed differences are not yet understood. There were two ionization processes observed in the Ar^{3+} cross section, the first peak is due to direct multiple ionization and the second peak is due to Auger processes.[24] There seems to be a clear indication that both ion optical effects and ion signal discrimination can play an important roll in the case of multiply charged ions. It appears to be essential to have the capability to vary the focusing properties of the mass spectrometer and to monitor the transmission theoretically by means of accurate ion trajectory calculations. We have demonstrated that our large opening angle time-of-flight apparatus with a very low discrimination setting can reliably measure the absolute partial ionization cross sections and these results would appear to cast doubt on the accuracy of previously reported absolute partial ionization cross sections for multiply charged species. In recent work in this laboratory on CF_4[33] we have arrived at a similar conclusion for cross sections of molecular ion fragments with several eV of translational kinetic energy.

Note added in proof. We have ruled out differing ion detector efficiencies as a source of the deviations in our results from those of others for Ar^{2+} and Ar^{3+}. The ratio I_{Ar}^{2+}/I_{Ar}^{+} was found to be independent of the detector impact energy from 2–4/4–8 keV for Ar^+/Ar^{2+}.

ACKNOWLEDGMENTS

The authors wish to thank the National Science Foundation for grant NSF PHY-8913096 which made this work possible. We also wish to thank the Chemistry Department's Electronic, Computer and Mechanical Instruments service groups. Special thanks are due William Miller who was primarily responsible for the construction of the apparatus and help with much of the mechanical design.

[1] G. Ecker and K. U. Riemann, Exp. Tech. Phys. **35**, 119 (1987).
[2] H. F. Winters, R. P. H. Chang, C. J. Mogab, J. Evans, J. A. Thornton, and H. Yasuda, Mater. Sci. Eng. **70**, 53 (1985).
[3] G. S. Oehrlein, Phys. Today **39**, 26 (1986).
[4] Y. Sakamoto, O. Matsumoto, S. Morita, S. Hattori, K. Fukimoto, Y. Ikada, E. Miyazaki, I. Kojima, and Y. Takahashi, *Japan Materials Report* (Japan Technical Information Service) (ASM International, Metals Park, OH, 1988).
[5] Ce Ma and R. A. Bonham, Phys. Rev. A **38**, 2160 (1988).
[6] R. R. Goruganthu and R. A. Bonham, Phys. Rev. A **34**, 103 (1986).
[7] R. R. Goruganthu, W. G. Wilson, and R. A. Bonham, Phys. Rev. A **35**, 540 (1987).
[8] R. K. Jones and R. A. Bonham, Aust. J. Phys. **35**, 559 (1982).

Downloaded 03 Mar 2008 to 203.230.125.210. Redistribution subject to AIP license or copyright; see http://rsi.aip.org/rsi/copyright.jsp

[9] H. Erhardt, K. Jung, R. Muller-Fiedler, and P. Schlemmer, Argonne National Laboratory Report, ANL-84-28 (1983).
[10] H. H. Willard, L. L. Merritt, Jr., J. A. Dean, and F. A. Settle, Jr., *Instrumental Methods of Analysis*, 6th ed. (Van Nostrand, New York, 1981).
[11] W. Bleakney, Phys. Rev. **36**, 1303 (1930).
[12] D. P. Stevenson and J. A. Hipple, Phys. Rev. **62**, 237 (1942).
[13] R. E. Fox, J. Chem. Phys. **33**, 200 (1960).
[14] F. Fiquet-Fayard, J. Chim. Phys. **59**, 439 (1962).
[15] F. Fiquet-Fayard and M. Lahmani, J. Chim. Phys. **59**, 1050 (1962).
[16] B. L. Schram, Physica **32**, 197 (1966).
[17] A. Gaudin and R. Hagemann, J. Chim Phys. **64**, 1209 (1967).
[18] M. J. Van der Wiel, Th. M. El-sherbini, and L. Vriens, Physica **42**, 411 (1969).
[19] S. Okudaira, Y. Kaneko, and I. Kanomata, J. Phys. Soc. Jpn. **28**, 1536 (1970).
[20] A. Crown, J. A. Preston, and J. W. McConkey, J. Chem. Phys. **57**, 1620 (1972).
[21] K. Stephan, H. Helm, and T. D. Märk, J. Chem. Phys. **73**, 3763 (1980).
[22] D. Mathur and C. Badrinathan, Int. J. Mass Spectrom. Ion Processes **57**, 167 (1984).
[23] R. C. Wetzel, F. A. Baiocchi, T. R. Hayes, and R. C. Freund, Phys. Rev. A **35**, 559 (1987).
[24] E. Krishnakumar and S. K. Srivastava, J. Phys. B **21**, 1055 (1988).
[25] Ce. Ma, Phillip B. Lieschеski, and R. A. Bonham, Rev. Sci. Instrum. **60**, 3661 (1989).
[26] D. A. Dahl and J. E. Delmore, "The SIMION PC/AT User's Manual, v.3.0," Idaho National Engineering Laboratory, EGG-CS-7233, 1987.
[27] R. R. Goruganthu and W. G. Wilson, Rev. Sci. Instrum. **55**, 2030 (1984).
[28] See AIP document No. PAPS RSINA-62-0909-9 for nine pages of electronic diagrams for the FASTMAC system. Order by PAPS number and journal reference from American Institute of Physics, Physics Auxiliary Publication Service, 335 East 45th Street, New York, NY 10017. The price is $1.50 for each microfiche (98 pages) or $5.00 for photocopies of up to 30 pages, and $0.15 for each additional page over 30 pages. Airmail additional. Make checks payable to the American Institute of Physics.
[29] D. Rapp and P. Englander-Golden, J. Chem. Phys. **43**, 1464 (1965).
[30] R. S. Gao, P. S. Gibner, J. H. Newman, K. A. Smith, and R. F. Stebbings, Rev. Sci. Instrum. **55**, 1756 (1984).
[31] J. B.Crooks and M. E. Rudd, Phys. Rev. A **3**, 1628 (1971).
[32] A. Müller, N. Djurić, G. H. Dunn, and D. S. Belić, Rev. Sci. Instrum. **57**, 349 (1986).
[33] Ce Ma, M. R. Bruce, and R. A. Bonham (to be published).

Downloaded 03 Mar 2008 to 203.230.125.210. Redistribution subject to AIP license or copyright; see http://rsi.aip.org/rsi/copyright.jsp